World Applied Sciences Journal 10 (Special Issue of Computer & Electrical Engineering): 10-19, 2010
ISSN 1818-4952

Dosimetry Study of Human Head Model for A Cellular Phone

[1]Mohammad Rashed Iqbal Faruque, [2]Mohammad Tariqul Islam and [3]Norbahiah Misran

[1]Department of Electrical, Electronic and Systems Engineering, Faculty of Engineering and Built Environment, Universiti Kebangsaan Malaysia, 43600 UKM, Bangi Selangor, Malaysia
[2]Institute of Space Science (ANGKASA),
Universiti Kebangsaan Malaysia, 43600 UKM, Bangi Selangor, Malaysia
[3]Department of Electrical, Electronic and Systems Engineering,
Faculty of Engineering and Built Environment, Institute of Space Science (ANGKASA),
Universiti Kebangsaan Malaysia, 43600 UKM, Bangi Selangor, Malaysia

Abstract: A dosimetric study in an anatomically realistic human head model for a helical antenna with mobile phone utilizing finite-difference time-domain (FDTD) method is adopted in this study. The method of SAR measurement is discussed and then the effects of head model size on SAR characteristics for a mobile phone exposure at 835 MHz respectively. The head model, was developed from magnetic resonance imaging (MRI) data of an adult head, consists of 630 thousand voxels, of 2 mm dimensions, segmented into 15 tissue types. The helical antenna was modeled as a heap of dipoles and loops with an enough relative weight, whose validity was established by comparing the calculated near magnetic fields with published measured data. SAR is given both for the spatial peak value in the whole head and the averages in various major organs.

Key words: Specific absorption rate (SAR) · Head size · Helical antenna · Finite difference time domain method (FDTD) · Electromagnetic dosimetry

INTRODUCTION

Health concern regarding the prospective danger that might be incurring due to the absorption of electromagnetic energy emitted by mobile phones has been growing. The truth that the transmitting antenna of a mobile phone is very close to the user's head when it's in use should come as no surprise. Henceforth, consideration of the potential health hazards due to this type of EM exposure is very important.

International Commission on Non-Ionising Radiation Protection (ICNIRP) [1] and IEEE [2] have set up revelation limits, defined in terms of basic restrictions, to defend the public and workers from probable hazards linked to electromagnetic-field overexposure. These basic limitations are safety limits that are based on established health effects. For the frequency between 100 kHz-10 GHz, these limits are defined by the specific absorption rate (SAR). Thus, the SAR analysis of wireless communications devices is decisive for dosimetric analysis, as well as for acquiescence assessment.

The growth of recent use and expected further increases in the use of cellular telephones and other personal communication services (PCS), there have been an interest and significant research endeavor loyal to interactions between antennas on handsets and the human body. These activities are provoked by two factors: I) a need to evaluate deterioration of the antenna performance and to develop better antennas [3-6]; and 2) a need to evaluate the rates of RF energy deposition, called specific absorption rates (SAR), in order to assess potential health effects and compliance with standards, e.g., the US. ANSI standard. Previous analyses ranged from those of simple models of the human head such as a homogeneous sphere, e.g., [5-7] or a homogeneous head shaped volume [6-9], to heterogeneous, anatomically correct models based on the magnetic resonance imaging (MRI) [l-3], [7-9]. Several studies dealt with a "generic" model of a cellular telephone at approximately 900 MHz consisting of a monopole on a metal box 15 cm long with a cross section of *5* to 6 cm by 1.3 to 2.5 cm [9-14]. A few commercially available telephones were analyzed, but details of their antenna type and box geometry were

Corresponding Author: Mohammad Rashed Iqbal Faruque, Department of Electrical, Electronic and Systems Engineering, Faculty of Engineering and Built Environment, Universiti Kebangsaan Malaysia, 43600 UKM, Bangi Selangor, Malaysia. Tel: +60102938061, E-mail: rashedgen@yahoo.com.

not given [8]. A few antenna designs, whose performance is less affected by the human head and which produce lower SAR in the head were also numerically modeled [15-17]. However, even for these antennas radiation patterns are significantly modified, usually in an undesirable way, by the user's hand.

There is, therefore, a great attention at the present time in the quite shorter helical antennas that can reduce significantly the length of the antenna, while providing radiation characteristics that are comparable to longer monopole antennas. For mobile telephones these antennas function in the so-called "normal mode," i.e., the maximum radiation is in a plane normal to the orientation of the antenna. Such a radiating mode has been studied in the literature [18-22]. It has been shown that for situations where the physical dimensions of the antenna (diameter and length) are much smaller than the wavelength, the helix can be approximated by a series of small loops and dipoles having diameter equal to the diameter of the helix and length equal to the pitch of the helix, respectively.

Since it allows inclusion of anatomically based head models, the finite-difference time-domain method (FDTD) [5-9] is currently the most used computational methods to calculate the rates of electromagnetic absorption [EM] in the human head due to cellular telephones [19-25]. The modeling of increasingly popular helical antennas has generally not been addressed in the literature even though it is possible to find alternative approaches that consider the model of thin loops and dipoles [24-26].

An approach to FDTD modeling of normal-mode helical antennas was recently proposed whereby the helical is approximated by a series of small loops and dipoles with source weights derived from analytical expressions for the helical far-fields [9-11]. Good agreement with experimental measurements for near electric field measurements, far-field radiation patterns and induced specific absorption rate (SAR) was reported. However, few dosimetric analyses have been addressed in the literature. This is because an obvious difficulty is the modeling of helical using usually rectangular FDTD cells. Lazzi and Gandhi have recently proposed a method to model a helical antenna as a stack of dipoles and loops, which does not need modification of the FDTD cell resolution to represent the helical or curved metal wires [9].

A dosimetric analysis is performed in a newly developed MRI-based head model for an actual mobile telephone with helical antenna in this paper. The mobile telephone is modeled as a plastic covered metal box and the helical antenna is modeled by using the Lazzi and Gandhi proposed method. The validity for the actual mobile telephone modeling is first confirmed by comparing the calculated near magnetic fields with measured data published in the literature. Then SAR are given both for the spatial peak value in the whole head and the averages in various major organs. Taking into consideration that a mobile telephone may not be adequately metalized a dosimetric analysis for a plastic covered abridged metal box with the same helical antenna is also carry out.

MATERIALS AND METHODS

The FDTD based electromagnetic simulation tool CST Microwave Studio was used to perform the dosimetry calculation. The software was explicitly developed for the analysis, optimization and synthesis of transceivers in the vicinity of lossy structures. A rectangular computational grid, based on the Yee cell, with a resolution of 1.25 mm and the total-field formulation have been used, while the perfectly matched layer (PML) absorbing boundary conditions with 8 PML has been employed [14-18]. The boundaries were placed 30 cells away from the nearest scattered. Converged results have been assured by using 12 time periods. The helical geometry has been approximated in the FDTD grid as a rectangular helical of wires using perfect conducting cell edges. The excitation has been modeled by imposing a harmonic voltage at a vertical one-cell feeding gap. The current flowing through the voltage source cell has been calculated by integrating the magnetic fields around the voltage source according to Ampere's law. The input impedance of the antenna has then been derived from the ratio of the voltage and the current together with their phase difference.

Averaged SAR over a reference mass (1gm or 10 gm) is calculated by an interpolation scheme. Cubical spaces centered on a cell are formed and the mass and average SAR of the sample cubes are found. The size of the sample cube increases until the total enclosed mass exceeds the reference mass. The sample cube increases in odd-numbered steps (1×1×1, 3×3×3, 5×5×5 etc) to remain centered on the desired cell. The cube may contain some non tissue cells, but it cannot contain an entire side or corner of non tissue cells. If the cube is found to be invalid, the averaging for the center cell stops and the same procedure is performed for the next center cell.

Head Models: In this study, we present a MRI-based, high-resolution, numerical model of the head of a healthy human subject. In order to devise the model,

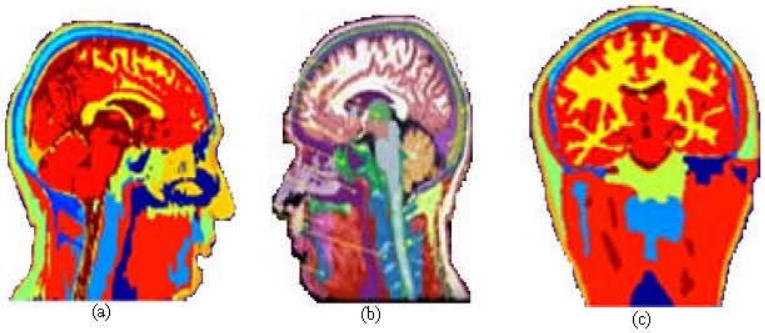

Fig. 1: MRI based human head model. (a) Appearance, (b) midsagittal vertical cross-section, (c) horizontal cross-section through the eyes

Table 1: Dielectric tissue properties at 835 MHz

Tissue	ρ [kg/m^3]	ε_r	σ [S/m]
Blood	1060	61.38	1.56
Bone	1850	16.68	0.25
Bone marrow	1030	11.31	0.24
Cartilage	1100	42.71	0.81
Cerebrospinal fluid	1010	68.67	2.44
Dura	1030	44.48	0.99
Eye tissue	1010	55.29	1.21
Fat	920	11.37	0.11
Grey matter	1030	52.76	0.96
Lens	1100	41.25	0.67
Mucous membrane	1010	46.12	0.88
Muscle	1040	55.99	0.99
Parotid gland	1050	60.75	1.24
Skin	1010	41.48	0.89
White matter	1030	38.96	0.61

we performed quantitative volumetric segmentation on the human head, using T1-weighted MRI. The high special resolution used ($1 \times 1 \times 1$ mm^3), allowed for the precise computation and visualization of a higher number of anatomical structures than provided by previous models. Furthermore, the high spatial resolution allowed us to study human being thin anatomical structures of clinical significance not visible by the standard model currently adopted in computational bioelectromagnetics. When we computed the electromagnetic field and specific absorption rate (SAR) at 7 Tesla MRI using the high-resolution model, we were able to obtain a detailed visualization of such fine anatomical structures as the epidermis/dermis, bone structures, bone-marrow, white matter and nasal and eye structures. An MRI based head mode laws utilized by software recently [12].The raw MRI data were taken from an adult head (male, 23 years old), which consists of 115 slices with 2mm apart in the axial plane. Each MRI slice was a 256× 256 pixel and 9-bit grey scale image. The grey scale data of MRI images were interpreted into tissue types, which are known as a process of segmentation. The segmented tissue types are blood, bone, bone marrow, cartilage, cerebrospinal fluid

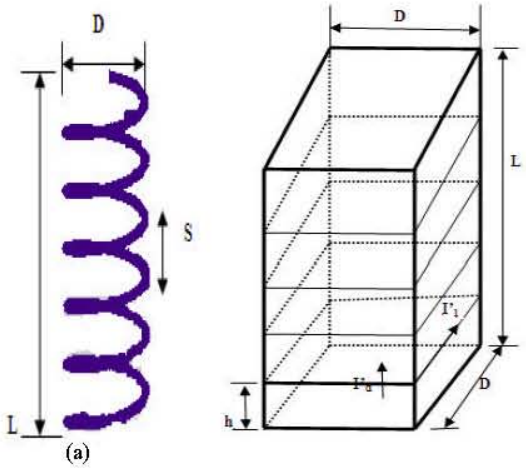

Fig. 2a-b: (a) The equivalence of a "normal mode" helical antenna in sequence of loops and dipoles (b) stack used to model the helical antenna. The stack is composed of several layers. Each layer has a square area with one side equal to the diameter D of the helical antenna, and a height h equal or close to the pitch S of the helical antenna. The height of the stack is equal to the length L of the helical antenna.

(CSF), dura, eye tissue, fat, grey matter, lens, mucous membrane, muscle, parotid gland, Skin and white matter.

Fig. 1 shows the head model, a midsagittal vertical cross-section and a horizontal cross-section through the eyes of the head model. The electrical properties for each tissue are cited from [13] and tabulated in Table 1, where ρ is the mass density and ε_r and σ are the relative permittivity and conductivity, respectively.

Helical Antennas with Mobile Phone: A small diameter (compared to wavelength) helical antenna working in the normal mode and a series of equivalent loops and dipoles are shown in Fig. 2(a) and (b), respectively.

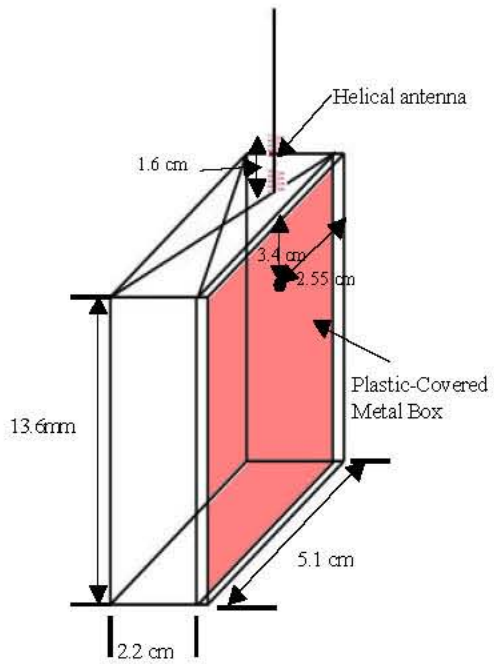

Fig. 3: Model of cellular phone with a helical antenna

A genuine 900 MHz mobile phone, reported in [11], was modeled by a helical antenna mounted on a plastic covered rectangular metal box. Fig. 3 shows the mobile telephone with a helical antenna model. The phone model metal box was 5.1 cm wide, 2.2 cm thick, 13.6 cm long and the covered plastic case had a thickness of 2 mm and $\varepsilon_r = 2$. The helical antenna had a length L =18 mm, pitch S=2 mm, diameter D=4 mm and was located at the onward side on the box. As in [17], the far field can be calculated, therefore, considering as source only one loop and one dipole. Defining ç as the characteristic impedance and k the propagation constant of the free-space, we can write.

$$E_\theta(r) = j\eta k I_d S \frac{\sin\theta}{4\pi r} e^{-jkr}. \quad (1)$$

$$E_\phi(r) = \eta k I_l S \frac{\pi^2 D^2}{2\lambda} \frac{\sin\theta}{4\pi r} e^{-jkr}. \quad (2)$$

Where, according to Fig. 2(a), D is the diameter of the helical antenna, S is the pitch and I_d, I_l are the currents passing, respectively, through the dipole and the loop. Therefore, in the far field we have

$$\frac{E_\theta}{E_\phi} = j\frac{I_d}{I_l}\frac{2S\lambda}{\pi^2 D^2} = j\frac{2S\lambda}{\pi^2 D^2}. \quad (3)$$

because of the continuity of the current $I_d = I_l$.

Fig. 2(b) shows that for one layer of the stack, there are an equivalent dipole and an equivalent loop. Denoting the current in the equivalent dipole as I_d', I_d' can be replaced by a displacement current and the equivalent electric field E_z in lieu of I_d' can be expressed as:

$$E_z = \frac{I_d'.1/j\omega C}{h} = \frac{I_d'}{j\omega\varepsilon_0 D^2} \quad (4)$$

Where, C is the capacitance between the layer, being given by $\varepsilon_0 D^2/h$ and h is the height of each layer.

On the other hand, denoting the current in the equivalent loop as I_l', from Ampere's law, the equivalent magnetic field related to the current I_l' in the center of the same layer can be expressed as.

$$H_Z = \oint \frac{I_l' dl' \sin\phi}{4\pi R^2} \approx \frac{I_l'}{D} \quad (5)$$

Where, R is the distance from the current element dl' to the center of the layer, ϕ is the angle between the direction of the current and the vector from the element to the center of the layer and the integration is carried out along the boundary line of the layer.

Thus, for one layer of the stack, we have.

$$\frac{E_z}{H_z} = \frac{I_d'}{I_l'}.\frac{1}{j\omega\varepsilon_0 D} \quad (6)$$

Since the stack has a rectangular shape and the height h of each layer may not be identical to the pitch of the helical antenna, it is necessary to relate the currents I_d' and I_l' to I_d and I_l produced by the actual dipole and loop. This was realized by scaling the dipole current by the ratio of the actual and modeled dipole length sand the loop current by the ratio of the actual and the modeled loop perimeters. Accordingly, we have,

$$I_d' = I_d\frac{S}{h} \text{ and } I_l' = I_l\frac{\pi D}{4D} \quad (7)$$

Thus Eq. (6) can be rewritten as

$$\frac{E_z}{H_z} = \frac{4S}{j\omega\varepsilon_0\pi h D} \quad (8)$$

Since $I_d = I_l$. This equation gives the relative weight between the electric and magnetic sources as the excitation.

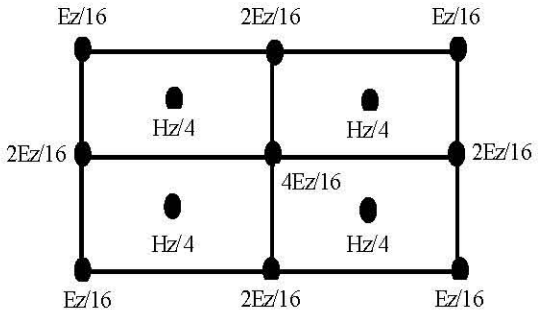

Fig. 4: The excitation method for each layer of the stack modeling the helical antenna

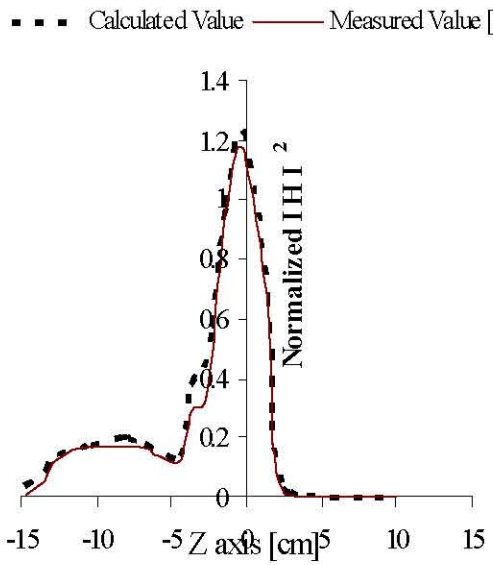

Fig. 5: Calculated and measured squared magnetic fields both normalized to the maximum field values at a distance of 5 mm from the phone model

It is straight forward to model the stack using FDTD cells. In this study, 2× 2 cells in the *xy* planes and 9 cells along the z direction were used to model the stack. That means that $S = h$ and $D = 2\delta$ in Eq. (5) where δ is the size of cubical FDTD cells. E_z and H_z in the cells modeling the stack were excited sinusoidally according to the relative weight in Eq. (5). Due to each layer of the stack consisted of four cells, the excitation with E_z and H_z was split and assigned as shown in Fig.4 according to Lazzi and Gandhi's proposal.

To confirm the validity of our modeling for the actual mobile telephone, the free space magnetic field H was calculated. Figure 5 shows calculated $|H|^2$ value at a distance of 5 mm from the cellular telephone. Also shown is the measured result reported in [11] by using a magnetic field probe. A good agreement was observed between them, though the calculated values were somewhat larger than the measured ones on the lower part of the box. This result assured that the model is a good representation of the actual portable telephone.

RESULTS AND DISCUSSION

All calculated results are analyzed in three sections. The antenna output power was set to 0.6 W, which was obtained from the sum of the power absorbed in the head and hand and the power radiated to the far field. The radiated power was calculated by integrating the normal component of the Pointing vector over a surface completely surrounding the configuration of analysis. The hand was simply modeled with 2/3 muscle equivalent material being 8 cm wide and 2 cm thick and wrapped around three sides of the lower part of the cellular telephone. The portable telephone had a vertical alignment at the side of the head by the ear.

Helical Antenna on a Plastic-Covered Metal Box: The magnetic field distribution as can be seen in Fig. 5, the helical antenna had stronger magnetic fields concentrated in the vicinity of the feed point. Also from Fig. 5, the helical antenna did not effectively choke the RF current on the box which is directly related to the near magnetic field [15]. This means that there may be an increased spatial peak SAR value in the head. Table 2 gives the SAR distributions for main organs in the MRI-based head model with the helical antenna on the plastic covered metal box. For comparison, the SAR distributions in the same MRI- based head model with a quarter-wavelength monopole antenna on a plastic covered metal box are also given. The quarter-wavelength monopole antenna had a radius of 0.48 mm and was located at the

Table 2: SAR distributions for MRI-based head model. The antenna output was 0.6 W

SAR [W/kg]	Helical	Quarter-wavelength monopole
1 gm peak SAR	2.006	1.75
10 gm peak SAR	1.16	0.82
Average SAR for whole head	0.048	0.047
1 gm peak SAR for brain	1.19	1.05
1 gm peak SAR for eye	0.022	0.032
Average SAR for grey matter	0.045	0.046
Average SAR for white matter	0.027	0.028
Average SAR for CSF	0.074	0.075
Average SAR for eye tissue	0.008	0.011
Average SAR for lens	0.002	0.005
Average SAR for parotid gland	0.119	0.087

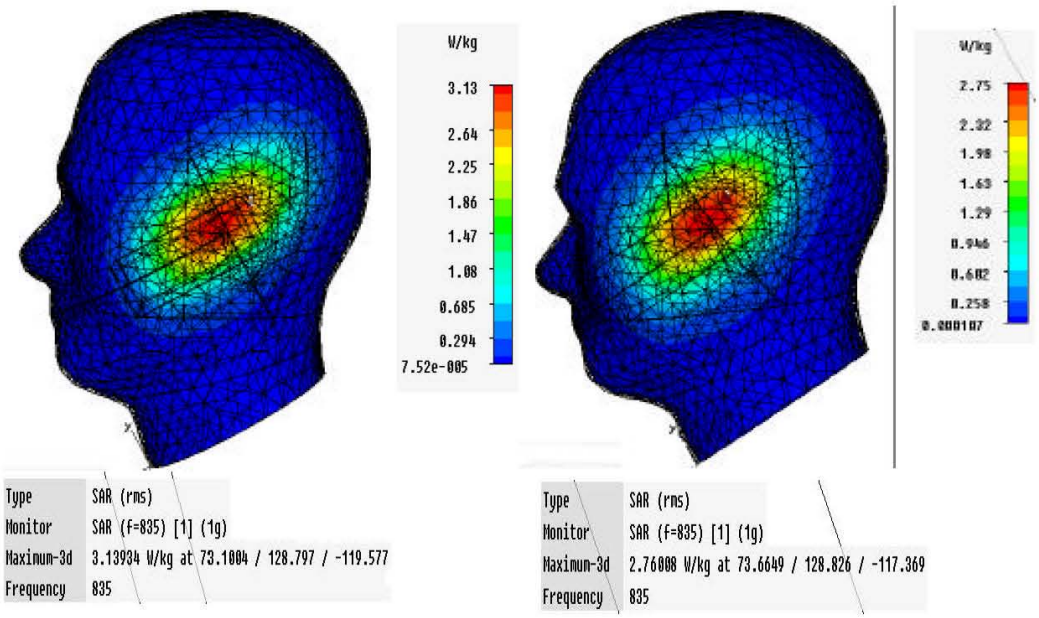

Fig. 6: SAR distributions on the head surface. (a) helical antenna, (b) quarter-wavelength monopole antenna. The antenna output was 0.6W

same location as that of the helical in Fig. 3. Both the 1 gm averaged and the 10 gm averaged spatial peak SAR were obtained over an exact 1 gm or 10 gm soft issue by using a linear interpolation scheme [18]. In addition, the 1 gm averaged spatial peak SAR for the brain was obtained over 1 gm of the grey matter, white matter and CSF and the 1 gm averaged spatial peak SAR for the eye was obtained over 1 gm of the eye tissue and lens. As expected, a raise in the 1 gm averaged and 10 gm averaged spatial peak SAR, say 1.1 times for the 1 gm average and 1.4 times for the 10 gm average, was observed with respect to the quarter-wavelength monopole. Moreover, the average SAR in the parotid gland was also increased significantly. But the average SAR in the major organs such as the brain and eyes were lower with respect to the quarter-wavelength monopole. This can be explained by comparing the SAR distributions on the head surface, as shown in Fig. 6, for the two different antennas. Due to the shorter length of helical antenna, the currents concentrated on the antenna and the upper part of the box, which resulted in a concentrated EM absorption in the face area touching the ear piece of telephone. However, with respect to the helical antenna, the peak values were lower but the exposed area was larger for the helical antenna. The exposed area for the helical antenna was somewhat on the low side relative to the auditory canal, while somewhat on the high side for the helical antenna that attributed to the increased average SAR level in the parotid gland and decreased average SAR level in the brain and eyes.

It is difficult to make a direct comparison for the spatial peak SAR with those reported in [8] because different helical sizes and different head models have been used. Lazzi and Gandhi have reported a 1 gm averaged spatial peak SAR of 3.9 W/kg at 835 MHz in [8]. This value is approximately 1.9 times our result at 835 MHz. The reason may be due to a shorter helical length and a pressed-ear head model used in their computation, because pressing the ear by a portable telephone would cause a significant increase in the spatial peak SAR [15].

Helical Antenna on a Plastic-covered Shortened Metal Box: In accuracy the plastic mobile telephone may not be sufficiently metalized to prevent EM fields penetrating the box. It is also possible that resonant elements may exist within the digital circuits of the device. In order to determine the effects that these circuits may have upon the SAR distributions a simulation using a shortened metal box has been carried out at 835 MHz. This box is of a similar size to that of the RF units inside a commercial mobile phone. A ë/4 monopole antenna and a helical antenna used in this study. However, the effect of shortening the box is more significant [19]. The shortened metal box may increase the field concentration

Table 3: SAR distributions for MRI-based head model with a helical antenna on a plastic covered shortened metal box. The antenna output was 0.6W

1 gm peak SAR	3.13
10 gm peak SAR	2.17
Average SAR for whole head	0.073
1 gm peak SAR for brain	2.27
1gm peak SAR for eye	0.032
Average SAR for grey matter	0.091
Average SAR for white matter	0.054
Average SAR for CSF	0.154
Average SAR for eye tissue	0.011
Average SAR for lens	0.032
Average SAR for parotid gland	0.074

surrounding the helical and the smaller box. Table 3 gives the SAR distributions for a helical antenna with mobile telephone with a plastic covered shortened metal box. The modeled mobile telephone had the same configuration and size as those in Fig. 3, except that the metal box was shortened to a height of 4.3 cm which was a similar size to a RF unit inside a portable telephone. From Table 3, a significant increase both in the peak SAR and average SAR were found with respect to the normal metal box model. The increased factors were 1.5 and 1.8 for the 1 gm averaged and 10 gm averaged spatial peak SAR. As an exception, the SAR level in the parotid gland was lower with respect to the normal metal box. This resulted from the highly field concentration and resultant smaller exposed for the portable telephone with the shortened metal box. For the cellular phone model with a normal metal box, about 33% absorbed power was due to the hand because a RF current flows on to that part of the box. However, for the mobile telephone model with the shortened metal box, only 17% absorbed power was due to the hand. The remaining part was absorbed in the head, which attributed to the increased average SAR in the head, brain and eyes. It should be noted that the radiation efficiency for the plastic covered cellular telephone model with a shortened metal box was deprived, say only 33%.

Fields in the Ear Canal: Electromagnetic fields are tremendously complicated, if not impracticable, to measure accurately in the ear canal using currently available field probes. Only computed fields can be used for comparison of their potency with levels of measured acoustic interference for hearing aids placed in the ear canal. Figs. 7 and 8 show the magnitude of the electric and magnetic fields for two models of the ear (pinna). These magnitudes are shown close to the center of the ear canal.

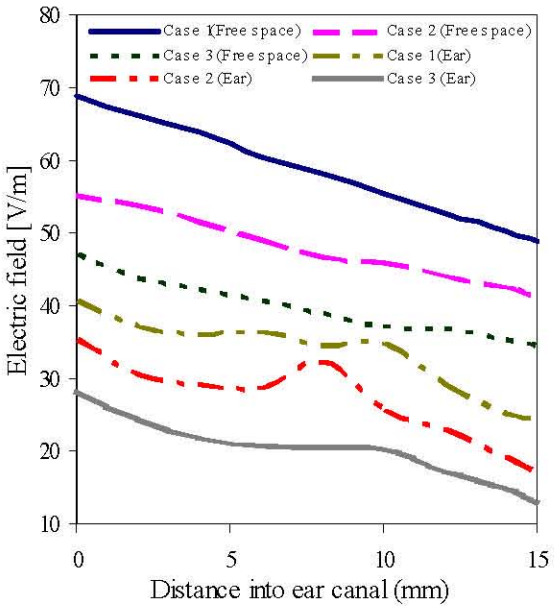

Fig. 7: Electric field magnitudes in free space and the ear canal for the compressed ear-model and various positions of the handset antenna. Case 1 & 4: the center of ear phone in the reference point. Case 2 & 5: the ear phone 5 mm away from the ear canal. Case 3 & 6: the ear phone 12 mm away from the ear canal, and aligned with the reference point.

It needs to be noted that the ear canal is not aligned with any axis of the coordinate system and does not proceed along a straight line. The distance shown on the abscissa is measured from an entrance into the auditory canal. The center of the entrance in the auditory canal is at the reference point. The magnitudes of the electric fields are attenuated in the ear canal, while the magnitudes of the magnetic fields are enhanced. The result for the magnetic field may be surprising; however, it is in agreement with the previously reported results for a monopole antenna on a handset [16]. The head in the near field of the handset antenna changes the input impedance and performance of the antenna. Further, the fields are scattered within the heterogeneous model of the head. As a result components of the field appear that are not present in free space electric field component may vary quite rapidly in the ear canal, as observed in [16], as well as in this paper. The magnitude of the total field usually changes more smoothly. A few rapid changes of the electric field in Figs. 7 and 9 are most likely due either to the test point being close to the canal wall or a rapid change in magnitude of one field component.

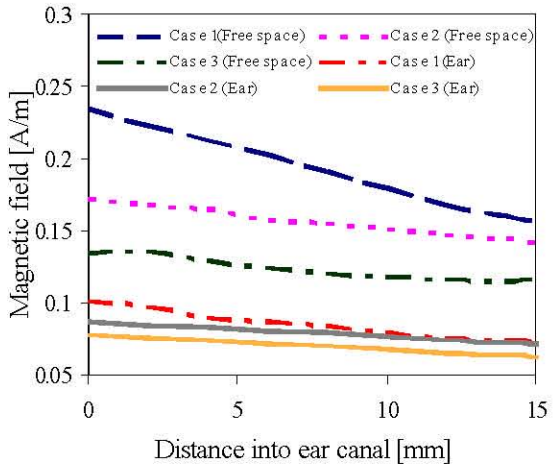

Fig. 8: Magnetic field magnitudes in free space and the ear canal for the compressed ear-model and various positions of the handset antenna. Case 1 & 4: the center of ear phone in the reference point. Case 2 & 5: the ear phone 5 mm away from the ear canal. Case 3 & 6: the ear phone 12 mm away from the ear canal, and aligned with the reference point.

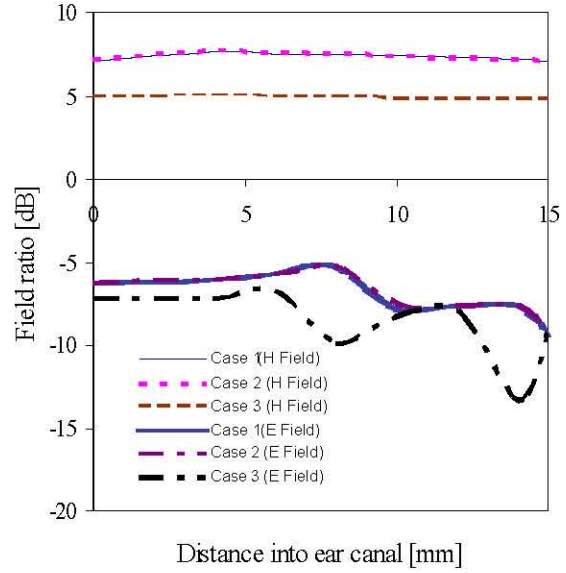

Fig. 9: Ratio of the electric fields (E) and Magnetic field in the ear canal to those in free space for the flattened ear model and various positions of the handset antenna. Case 1: the center of earphone in the reference point. In Fig. 2 (c) B: the earphone 4 mm away from the ear canal, and aligned with the reference point. C: the earphone 12 mm away from the ear canal, and aligned with the reference point.

Certain self-consistent features of the field behavior in the ear canal can be observed. One of them is that, for the electric fields, the order of the curves for the field magnitude in the ear canal, in general, corresponds to that of the field magnitude in free space. The relationship is not evident to the same extent for the magnetic fields, but generally reasonable. The behavior of the magnetic fields is reasonable in view of the free-space field distribution

CONCLUSIONS

A novel method to model helical antennas and usually antennas involving helical components has been analyzed. The helical antenna has been modeled as a stack of dipoles and loops with an adequate relative weight. As a result, a higher 1 gm averaged or 10 gm averaged spatial peak SAR has been found with respect to a quarter-wavelength monopole antenna, while lower average SAR has been found in the main organs such as the brain and eyes except for the parotid gland. The increased SAR values can be explained by the field concentration surrounding the shorter helical antenna. A plastic covered shortened metal box has exhibited a stronger field concentration effect, which results in an additional increase on the spatial peak SAR in the ear area as well as the SAR values in the brain and eyes. In addition, the electric and magnetic fields inside the auditory canal have also been investigated. The dominant component of electric field exhibits a standing-wave characteristic, while the magnetic field strength decreases with the distance away from the entrance of auditory canal quite slowly.

ACKNOWLEDGEMENT

The authors would like to thank Institute of Space Science (ANGKASA), Universiti Kebangsaan Malaysia (UKM) and the MOSTI Secretariat, Ministry of Science, Technology and Innovation of Malaysia, e- Science fund: 01-01-02-SF0612, for sponsoring this work.

REFERENCES

1. IEEE C95.1, 2005. IEEE standards for safety levels with respect to human exposure to radio frequency electromagnetic fields, 3 kHz to 300 GHz, Institute of Electrical and Electronics Engineers, New York, NY, 2005.

2. International Non-Ionizing Radiation Committee of the International Radiation Protection Association, Guidelines on limits on exposure to radio frequency electromagnetic fields in the frequency range from 100 kHz to 300 GHz, Health Physics, 54(1): 115-123, 1988.
3. Al-Sharaeh, S.H., A.A. Sharieh, A. Latif Abu Dalhoum, R. Hosny and F. Mohammed, 2008. Multi-dimensional Poisson distribution heuristic for maximum lifetime routing in wireless sensor network, World Applied Sciences J., 5(2): 119-131.
4. Ebrahimi-Ganjeh, M.A. and A.R. Attari, 2007. Interaction of dual band Helical and PIFA handset antennas with human head and hand Progress In Electromagnetics Res. PIER, 77: 225-242.
5. Naghipour, M., H.M. Daniali and S.H.A. Hashemi Kachapi, 2008. Numerical simulation of composite plates to be used for optimization of mobile bridge deck," World Applied Sci. J., 4(5): 681-690.
6. Islam, M.T., M.R.I. Faruque and N. Misran, 2010. Study of specific absorption rate (SAR) in the human head by metamaterial attachment, IEICE Electronics Express, 7(4): 240-246.
7. Balzano, Q., O. Garay and T.J. Manning Jr,1995. Electromagnetic energy exposure of simulated users of portable cellular phones, IEEE Trans. Vehicular Technol., 44: 390-403.
8. Faruque, M.R.I., M.T. Islam and N. Misran, 2010. Evaluation of specific absorption rate (SAR) reduction for PIFA antenna using metamaterials, Frequenz J., 64(7-8): 1-6.
9. Lazzi, G. and O.P. Gandhi, 1998. On modeling and personal dosimetry of cellular telephone helical antennas with the FDTD code, IEEE Trans. Antennas Propagat., 46: 525-530.
10. Babazadeh, F. and S.H. Keshmiri, 2009. Modeling of a novel high-Q, highly linear, if micromechanical filter: design and simulations, World Appl. Sci. J., 6(7): 914-925.
11. Hombach, V., K. Meier, M. Burkhardt, E. Khun and N. Kuster, 1996. The dependence of EM energy absorption upon human head modeling at 900 MHz, IEEE Trans. Microwave Theory and Tech., 44(10): 1865-1873.
12. Khan, S., R. Farooq, S. Shahbaz, M. Aziz Khan and M. Sadique, 2009. Health risk assessment of heavy metals for population via consumption of vegetables, World Applied Sci. J., 6(12): 1602-1606.
13. Gabriel, C., 1996. Compilation of the dielectric properties of body tissues at RF and Microwave frequencies, Brooks Air Force Technical Report Al/OE-TR-1996-0037.
14. Islam, M.T., M.R.I. Faruque and N. Misran, 2009. Design analysis of ferrite sheet attachment for SAR reduction in human head," Progress In Electromagnetics Research, PIER, 98: 191-205.
15. Islam, M.T., M.R.I. Faruque and N. Misran, 2009. Reduction of specific absorption rate (SAR) in the human head with ferrite material and metamaterial, Progress In Electromagnetics Research, PIER C, 9: 47-58.
16. Okoniewski, M. and M.A. Stuchly, 1998. Modeling of interaction of electromagnetic fields from a cellular telephone with hearing aids," IEEE Trans. Microwave Theory and Tech., 46(11): 1686-1693.
17. Koulouridis, S. and K.S. Nikita, 2004. Study of the coupling between human head and cellular phone helical antennas, IEEE Trans. on Eectromag. Compa., 46(1): 62-70.
18. Wang, J. and O. Fujiara, 1999. Uncertainty of the one-gram averaged spatial peak SAR in human head for portable telephones due to average procedures, Trans. IEE of Japan, 119(1): 2-8.
19. Tinniswood, A.D., C.M. Furse and O.P. Ghandhi, 1998. Computations of SAR distributions for two anatomically based models of the human head using CAD files of commercial telephones and parallelized FDTD code," IEEE Trans. Antennas and Propag., 46(6): 829-833.
20. Arenas, J.J., J. Anguera and C. Puente, 2009. Balanced and single-ended handset antennas: Free space and human loading comparison," Microwave and Optical Technol Letts., 51(9): 2248-2254.
21. Wong, M. and J. Wiart, 2005. Modeling of electromagnetic wave interactions with the human body, C. R. Physique, 6(6): 585-594.
22. Bank and B. Levin, 2007. The Development of a Cellular Phone Antenna with Small Irradiation of Human-Organism Tissues," IEEE Antennas and Propagation Magazine, 49(4): 65-73.
23. Christopoulou, M., S. Koulouridis and K.S. Nikita, 2009. Parametric study of power absorption patterns induced in adult and child head models by small helical antennas" Progress In Electromagnetics Res. PIER, 94: 49-67.

24. Kouveliotis, N.K., S.C. Panagiotou, P.K. Varlamos and C.N. Capsalis, 2006. Theoretical approach of the interaction between a human head model and a mobile handset helical antenna using numerical methods Progress In Electromagnetics Research, PIER, 65: 309-327.
25. Dimbylow, P.J., 1997. FDTD calculations of the whole body averaged SAR in an anatomically realistic voxel model of the human body from 1 MHz to 1 GHz, Phys. Med. Biol., 42: 479-490.
26. Shaukat, S.F., M.I. Ansari, R. Farooq, U. Ibrahim and M. Faisal, 2009. Mobile phone location determination in urban and rural areas using enhanced observed time difference technique, World Appl. Sci. J., 6(7): 902-907.